JTTEE5 10:502-510

Sliding Wear Behavior of Tungsten Carbide Thermal Spray Coatings for Replacement of Chromium Electroplate in Aircraft Applications

A.C. Savarimuthu, H.F. Taber, I. Megat, J.R. Shadley, E.F. Rybicki, W.C. Cornell, W.A. Emery, D.A. Somerville, and J.D. Nuse

(Submitted 19 September 2000)

Tungsten carbide (WC) thermal spray coatings have gained increased acceptance for commercial aircraft applications driven by the desire to replace chromium electroplate due to environmental and economic considerations. In order to confidently replace electroplated chrome with WC thermal spray coatings in aircraft applications, the coatings must demonstrate fatigue and wear characteristics as good as or better than those of electroplated chrome. Previous research in this area has shown that the fatigue life of the WC thermal spray coatings can be improved by inducing compressive residual stresses in the coating. This paper compares the wear characteristics of several types of WC thermal spray coatings with those of electroplated chrome in sliding wear tests using the "block-on-ring" procedures described in the ASTM G77 standard. Wear results are interpreted in terms of coating residual stresses and in terms of x-ray diffraction (XRD) and scanning electron microscope (SEM) analyses.

Keywords aircraft landing gear, ASTM G77, chrome plating, HVOF, residual stress, tungsten carbide, wear

1. Introduction

Electroplated chrome and hard anodizing are currently employed in surface engineering practice. Two important reasons for applying these surface enhancement processes are to increase the wear resistance and corrosion resistance of aircraft components. However, the detrimental environmental aspects of electroplated chrome[1] have generated a search in the aircraft industry for alternatives to chrome plating. Over the past decade, tungsten carbide (WC) coatings applied by the HVOF process have emerged as one of the most promising alternatives to electroplated chrome.[2] One objective of this paper is to compare the wear characteristics of several WC thermal spray coatings with those of electroplated chrome applied against standard commercial aircraft bearing materials and against themselves.

2. Objectives

In this research, selected characteristics of WC thermal spray coatings are examined to provide information toward understanding whether the coatings are suitable candidates for replacement of electroplated chrome in aircraft and helicopter applications such as landing gear. Specific objectives are to (1) compare wear characteristics of WC thermal spray coatings with those of chrome plating when applied against two standard commercial aircraft materials and against themselves, (2) evaluate the residual stresses in the different coatings and relate the results to the wear characteristics of the respective coatings, and (3) examine relationships between wear characteristics of the different WC coatings and the phase composition and microstructures of the coatings.

A.C. Savarimuthu, H.F. Taber, I. Megat, J.R. Shadley, E.F. Rybicki, and **W.C. Cornell,** The University of Tulsa, Tulsa, OK 74104; and **W.A. Emery, D.A. Somerville,** and **J.D. Nuse,** Southwest Aeroservice, Inc., Tulsa, OK 74120. Contact e-mail: john-shadley@utulsa.edu.

3. Experimental Procedures

Descriptions of the experimental procedures are presented below for (1) sliding wear tests, (2) evaluation of residual stresses in the coatings, (3) x-ray diffraction (XRD) analysis, (4) microstructural examination of the coatings, (5) evaluation of Young's modulus of the coatings, and (6) evaluation of the microhardness of the coatings.

3.1 Procedure for Sliding Wear Tests

The ASTM G77 "block-on-ring" standard test[3] was used to study the sliding wear characteristics of different WC thermal spray coatings and electroplated chrome. The ASTM G77 block-on-ring standard test encompasses procedures beyond the scope of this paper; therefore, only a subset of its procedures was used. According to ASTM G77 Section 4.1, the block-on-ring test is performed as follows: "A test block is loaded against a test ring that rotates at a given speed for a given number of revolutions. Block scar volume is calculated from the block scar width, and ring volume loss is calculated from ring weight loss. The friction force required to keep the block in place is continuously monitored during the test with a load cell." A schematic of the ASTM G77 test configuration is shown in Fig. 1.

3.2 Wear Test Machine

The wear test machine used in this research is shown in Fig. 2. The machine has a dual test station setup, whereby two sets of specimens can be run simultaneously on opposite ends of a cen-

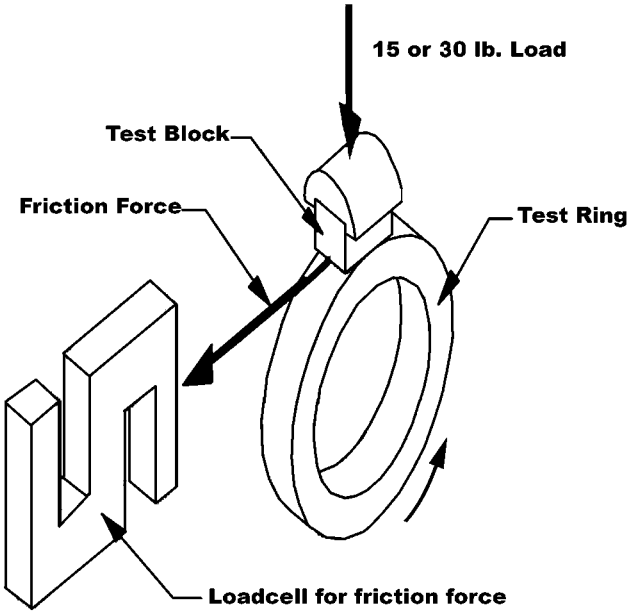

Fig. 1 ASTM G77 schematic

Table 1 Block materials tested

	Block material/coating
1	Al-Ni-Bz AMS 4640 (no heat treatment)
2	Cu-Be AMS 4533 (no heat treatment)
3(a)	Plasma 88WC-12Co
4(a)	HVOF 88WC-12Co
5(a)	HVOF 83WC-17Co tensile residual stress
6(a)	HVOF 86WC-10Co-4Cr
7(a)	Chromium electroplate
8(a)	HVOF 83WC-17Co high stress(b)
9(a)	HVOF 83WC-17Co low stress(b)

(a) For blocks 3 to 9, the base material was AISI 4130 steel
(b) High and low stress refer to target levels of compressive residual stresses in these coatings

trally driven shaft. One station was set up for a 6.8 kg load and the other for a 13.6 kg load. Each test station was calibrated and dead weight tested for load accuracy. All testing was performed at a ring rotation speed of 83 rpm. The normal span of the test was 30 min, except for the self-tests (coating on coating), which were carried out for 120 min.

Lubrication was supplied continuously by two spring-loaded grease cups. Boeing Material Standard (BMS) 3–33[4] specification grease was used with all samples. Two 0.0 to 2.25 kg load cells were used to record the friction force. The friction load was recorded every 6 s throughout the test.

Pre-Test Specimen Preparation. *Blocks:* Test blocks were 15.75 × 10.16 × 6.35 mm and machined to tolerances per G77 specifications. The roughness of the block surfaces before testing was measured to be within the range of 0.025 to 0.102 μm Ra. Coating thickness after grinding was 0.076 to 0.127 mm. Block materials and coatings used in the research are listed in Table 1.

Rings: The outside diameters of the test rings were cylindrically ground to the test diameter of 35 mm. The roughness of the ring surfaces before testing was measured to be within the range of 0.406 to 0.813 μm Ra. Coating thickness after grinding was 0.076 to 0.127 mm. The initial diameter and the initial ring weights were measured. The ring coating materials are listed in Table 2.

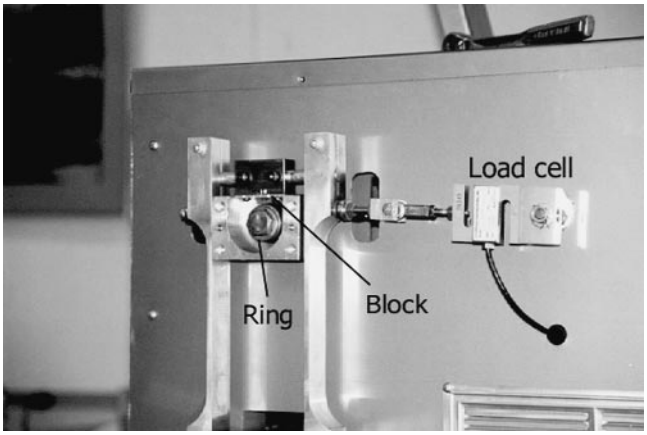

Fig. 2 Sliding wear test machine

Table 2 Ring materials tested

	Ring coating material(a)
1	Plasma 88WC-12Co
2	HVOF 88WC-12Co
3	HVOF 83WC-17Co tensile residual stress
4	HVOF 86WC-10Co-4Cr
5	Chromium electroplate
6	HVOF 83WC-17Co high stress(b)
7	HVOF 83WC-17Co low stress(b)

(a) The base material for all rings was SAE 4620 steel
(b) High and low stress refer to target levels of compressive residual stresses in these coatings

Test Procedure. All the blocks and rings were cleaned prior to testing. The test ring was mounted in the test machine on a tapered spindle and held in place with a machine bolt. The block was mounted in the self-centering housing above the ring and the alignment of the block to the ring was inspected. Spring-loaded grease cups constantly fed fresh grease directly onto the ring. The test was started and run continuously until completion. After the completion of the test, the blocks and rings were cleaned to remove all test grease and other residue before any measurements or weights were recorded.

Data Recorded. *Ring:* Changes in ring weight ($\pm$1.0 mg) and ring diameter ($\pm$13.0 μm) were measured to determine the amount of material transferred.

Block: Scar width was measured using a 60× micrometer microscope. Volume loss was calculated from the block scar width according to the ASTM G77 procedure. For scar widths typical for test blocks made of aircraft bearing materials, the volume loss error is less than $\pm$1.5%. For scar widths typical for thermal spray coated blocks, the volume loss error is less than $\pm$6.0%.

Frictional force: Data acquisition software displayed and recorded friction force ($\pm$0.1 N) versus time during the test.

3.3 Procedure for Evaluating WC Coating Residual Stresses

Residual stress specimen description: The original dimensions and materials of the residual stress specimens are shown in

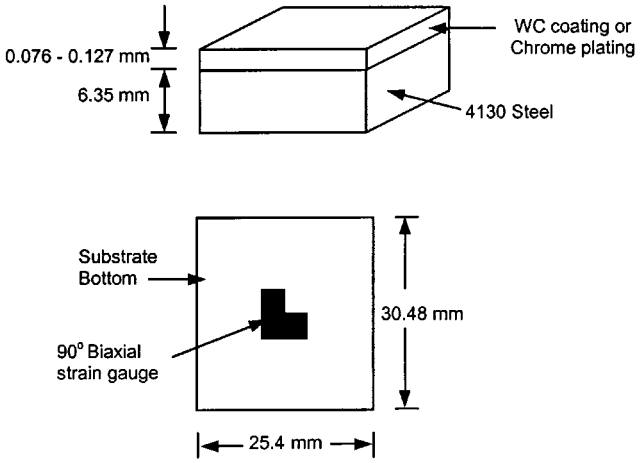

Fig. 3 Residual stress specimen dimensions

Table 3 Types of coating material

	Residual stress specimen coating material(a)
1	Plasma 88WC-12Co
2	HVOF 88WC-12Co
3	HVOF 83WC-17Co tensile residual stress
4	HVOF 86WC-10Co-4Cr
5	Chromium electroplate
6	HVOF 83WC-17Co high stress(b)
7	HVOF 83WC-17Co low stress(b)

(a) The base material for all the specimens was AISI 4130 steel
(b) High and low stress refer to target levels of compressive residual stresses in these coatings

Fig. 3. Dimensions of 25.4 × 30.5 × 6.35 mm thick were used for the substrate. The different types of WC thermal spray coatings for residual stress measurements are listed in Table 3. The substrate surfaces were grit blasted prior to being coated with the thermal spray coating. The HVOF WC thermal spray coatings were sprayed using Jet Kote® II HVOF spray equipment (Stellite Coatings, Goshen, IN). The final coating thickness was 0.076 to 0.127 mm. After coating, the sides of the specimen were polished to remove any overspray. The roughness of the coating surfaces was measured to be within the range of 0.406 to 0.813 μm Ra. Metco AP sealer (Sulzer Metco Inc., Westbury, NY) was used to seal the coatings. Plasma-sprayed coatings were applied using a Miller Model SG-100 plasma spray gun (Praxair Surface Technologies/TAFA Inc., Concord, NH). The chrome plating was applied according to the U.S. Military Plating Specification QQ-C-320.[5]

3.4 Residual Stress Measurements

The modified layer removal method (MLRM)[6] was used to determine the through-thickness residual stress distributions in the coatings and chrome plating. The procedure involved mounting biaxial strain gauges to the uncoated side of the residual stress specimen and removing thin layers of the coating or chrome plating until all coating was removed. Layers 0.025 to

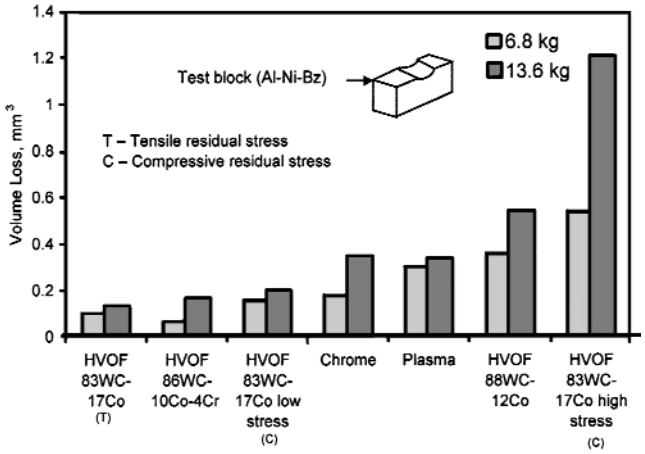

(a)

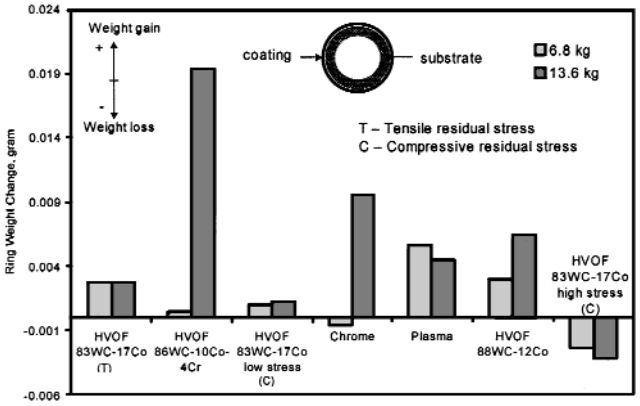

(b)

Fig. 4 Wear test results for coated rings against Al-Ni-Bz blocks: (**a**) block volume loss and (**b**) ring weight change

0.050 mm in thickness were removed in each step. The layer removal procedure was performed using a metallurgical polishing wheel. Thickness measurements of the specimen were made after each layer was removed.

Changes in strain gauge readings due to each layer removal were recorded. Strain and thickness changes are input to a residual stress analysis back-computation procedure defined by the MLRM. The analysis is applied to each layer removed and calculates the residual stress in the layer removed and the change in stress distribution for the remaining piece. The stresses are summed in the back-computation procedure for each layer removed to compute the residual stresses that existed in the specimens before any material was removed.

3.5 XRD to Characterize Chemical Composition of Powders

The three powders used to produce the coatings are listed in Table 4. X-ray diffraction analysis was performed on the powders to determine the characteristics of the powder before spraying. There was no evidence of W_2C or W in the powders, so the presence of W_2C or W would be a result of decarburization re-

Table 4 Feedstock powder characteristics

Powder	Company address	Composition	Manufacturing process morphology	Particle size, μm
H.C. Stark, Amperit® 526.062	H.C.Stark Inc., 45 Industrial Place, Newton, MA 02161-1951	83WC-17Co	Agglomerated and sintered	−53/+10
H.C.Stark, Amperit® 518.28	H.C.Stark Inc., 45 Industrial Place, Newton, MA 02161-1951	88WC-12Co	Agglomerated and sintered	−45/+15
Praxair AI-1186	Praxair Surface Technologies/TAFA Inc., 146 Pembroke Road, Concord, NH 03301	86WC-10Co-4Cr	Sintered and crushed	−45/+15

actions during deposition. The spray processes used for the residual stress specimens were also used for the XRD analysis specimens.

The phase compositions of the feedstock powders and of the sprayed coatings were investigated by x-ray diffraction using CuK_α radiation in the range $2\theta = 10$ to 80°. No W_2C or W appeared in the feedstock powders. Thus, the ratio of W_2C to WC (W_2C peak at $d = 2.275$ Å [39.6°, 2θ] and WC peak at $d = 1.884$ Å [48.3°, 2θ]) could be used as an indication of the extent of powder decarburization during spraying.

3.6 Scanning Electron Microscope

To investigate coating porosity and the density of WC particles in the coatings, polished sections were examined with the SEM and an energy-dispersive x-ray spectrometer. Secondary electrons were used for the SEM analysis.

3.7 Procedure for Evaluating Elastic Modulus and Microhardness of Coatings

The cantilever bending beam method (CBBM) was used to determine the Young's modulus (E_c) of the coating.[7] The CBBM is a static deflection method for determining E_c. The analysis is based on elastic stress-strain analysis of a two material composite beam. The method involves mounting two biaxial resistance strain gauges, one on the coating side and the other on the substrate side, directly opposite the coating biaxial gauge. One end of the beam is fixed in a vise. Weights are added to the free end of the cantilever beam to load the gauged sections in a known bending moment. The coating is assumed to be isotropic in the plane of the coating. The largest applied stress is in the direction of the length of the cantilevered beam; but, there are also transverse stresses in the coating due to the different Poisson's ratio between the coating and the substrate. The strain readings and bending loads are provided as input to a computer program that computes E_c based on the deformations of the strain gauges and the applied bending moment at the gauged section. The elastic modulus of the coating in tension and the elastic modulus of the coating in compression were then determined.

Microhardness tests were performed on the polished coating cross sections using a diamond pyramid indentor and a load of 500 g force. Tests were performed at six locations on one specimen of each coating type.

4. Results and Discussion

4.1 Wear Test Results

Coatings tested against Al-Ni-Bz blocks: Superior or highly desirable wear characteristics of a block and ring set are characterized by a small block scar width with very little loss or gain of the ring material. Inferior wear characteristics would exhibit a badly worn block and a ring with an excessive amount of material loss or gain.

Figure 4 represents the wear test results on aluminum-nickel-bronze (Al-Ni-Bz) blocks tested against the various coated rings. Figure 4(a) shows the block scar volume, while Fig. 4(b) shows the ring weight change. From Fig. 4(a), it can be seen that three WC coatings removed less bearing material from blocks than chrome plating, while three coatings removed more. The 83WC-17Co coating with a tensile residual stress target removed the least amount of bearing material from the Al-Ni-Bz blocks tested under high (13.6 kg) load. The coating producing the lowest amount of block wear tested under low (6.8 kg) load was the 86WC-10Co-4Cr coating. However, from Fig. 4(b), one can see that, under high load, the ring with the 86WC-10Co-4Cr coating picked up more material from the block than any other coating. The 83WC-17Co with a low compressive residual stress level exhibited small block wear under both low and high load, and had the least amount of material transfer from the block to the ring. This suggests that the low compressive residual stress 83WC-17Co coatings provide good wear characteristics for both high and low test load conditions.

The electroplated chrome specimens proved to work better under lower test load applications. For the higher test load, the block material picked up by the chrome-plated ring was very high and was exceeded only by the 86WC-10Co-4Cr coating. Although less material was transferred to the 88WC-12Co plasma-coated rings, a considerable amount of block material was removed during this test. The 88WC-12Co HVOF coating proved to have a significant amount of block wear when compared to other coatings. The high compressive residual stress 83WC-17Co coated rings resulted in the highest block wear rate among all the tested coatings and also showed significant ring weight loss.

Coatings tested against Cu-Be blocks: Figure 5 shows the block volume loss and ring weight change data for various ring materials tested against copper-beryllium (Cu-Be) blocks. When the coatings were tested against Cu-Be blocks, two of the WC

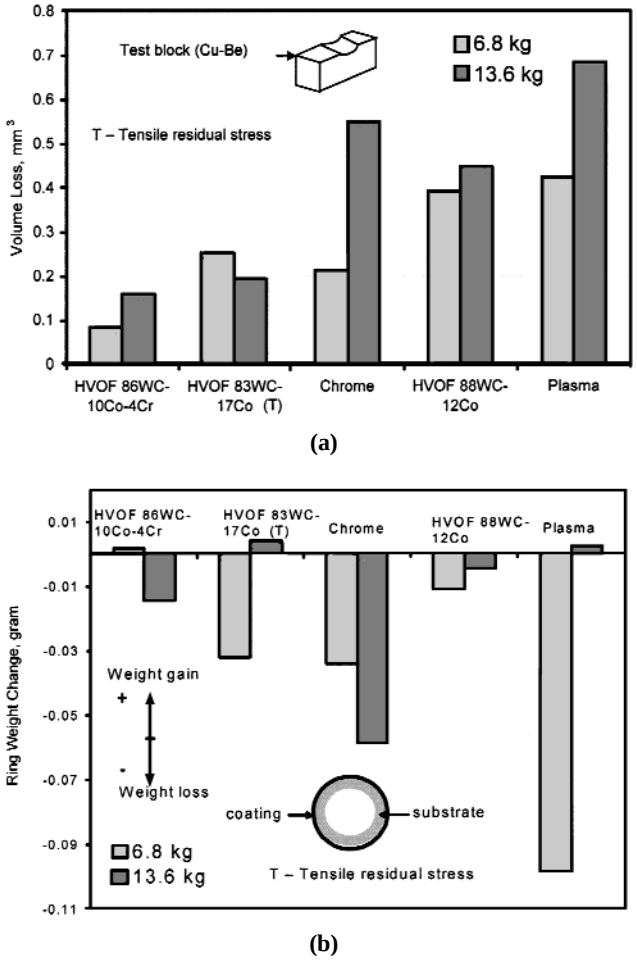

Fig. 5 Wear test results for coated rings against Cu-Be blocks: (**a**) block volume loss and (**b**) ring weight change

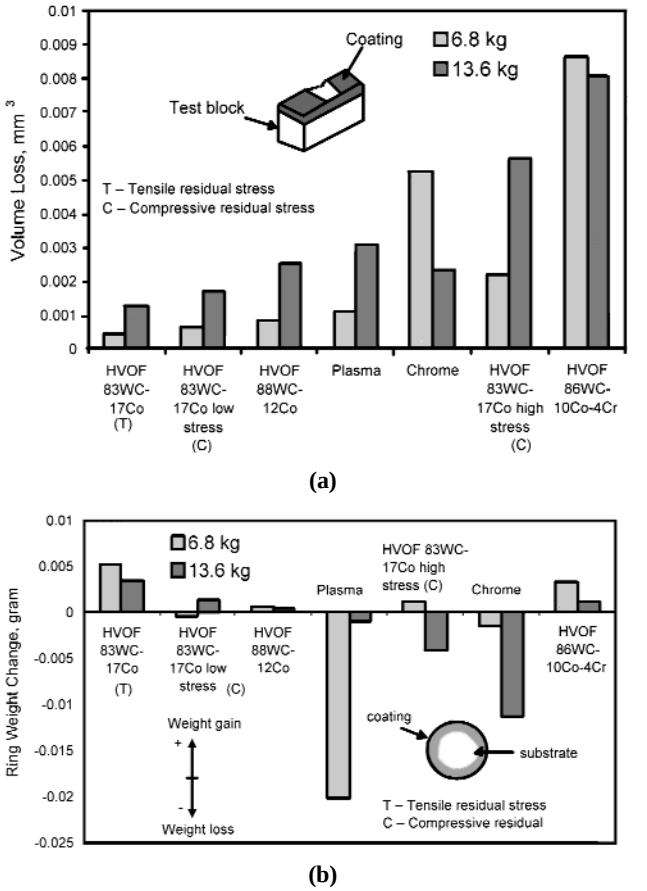

Fig. 6 Wear test results for coated rings against coated blocks (self-tests): (**a**) block volume loss and (**b**) ring weight change

coatings tested removed less bearing material than chrome plating, while two WC coatings removed more. The 86WC-10Co-4Cr coating exhibited the best wear characteristics at the high and low test loads. The coating producing the second lowest block wear was the HVOF 83WC-17Co coating with tensile residual stress target.

The 88WC-12Co HVOF coating did not perform well when tested against the Cu-Be blocks. Block wear was higher for this coating than for any other coating except the plasma-sprayed coating. However, this coating revealed very little wear on the ring. The worst performer against the Cu-Be blocks was the 88WC-12Co plasma-sprayed coating that showed significant block wear under both low and high load tests. The rings with electroplated chrome also lost a significant amount of material under both low and high load test conditions.

Coatings tested against coating (self-tests): In this series of tests, the coated rings were tested against blocks with the same coatings, a hard surface against a hard surface. These tests were originally run at the planned 30 min time limit, but block scars were small and irregular, so the time limit for the test was increased to 120 min.

Figure 6 shows the block volume loss and ring weight change data for coated blocks and coated rings. From Fig. 6(a), it can be seen that four of the six coatings tested out performed chrome plating on block volume loss. The 83WC-17Co coated rings with tensile residual stress target removed the least amount of material from the similarly coated blocks under both test load conditions. But the ring having the 83WC-17Co tensile residual stress target coating had a substantial amount of weight gain for both the loads. The coating with the second lowest block material loss was the low compressive residual stress 83WC-17Co coating. The ring weight change for the 83WC-17Co low compressive residual stress coating shown in Fig. 6(b) was not significant.

The HVOF 88WC-12Co coating proved to perform better in wear against itself when compared to the 88WC-12Co plasma and high compressive residual stress 83WC-17Co coatings. The 88WC-12Co plasma coating had maximum ring weight loss under low load conditions. Among the coatings tested, the 86WC-10Co-4Cr coating had the highest wear under both the high and low load test conditions.

4.2 Through-Thickness Residual Stress Distributions

Through-thickness residual stress distributions for each of the thermal spray coatings and chrome plating were determined using the MLRM.[6] Figure 7 shows plotted residual stress dis-

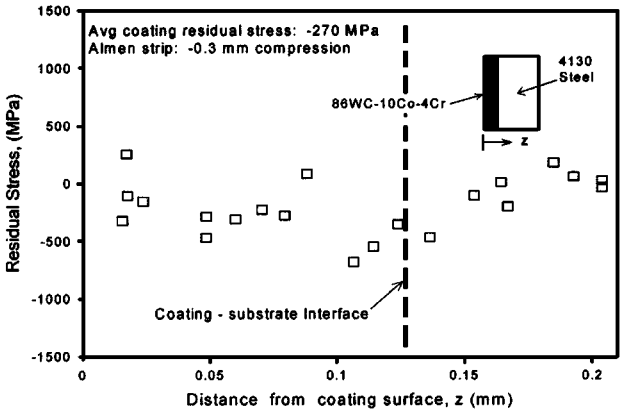

Fig. 7 Through-thickness residual stress distribution for 86WC-10Co-4Cr coated specimens

Table 5 Average residual stresses in the coatings(a)

Coating material	Average residual stress, MPa	Almen strip results, mm
86WC-10Co-4Cr	270 (C)	0.305 (C)
83WC-17Co (high compressive residual stress)	169.3 (C)	0.114 (C)
88WC-12Co HVOF	138 (C)	0.089 (C)
83WC-17Co (low compressive residual stress)	100 (C)	0.089 (C)
83WC-17Co (tensile residual stress)	71 (T)	0.051 (T)
88WC-12Co plasma	160 (T)	0.139 (T)
Chrome	234 (T)	…

(a) T—tension, and C—compression

tribution data for four specimens having the 86WC-10Co-4Cr coating. Similar plots were constructed for the other coatings and chrome plating.

Average Coating Residual Stress Levels: The average residual stress in the coating, $\bar{\sigma}$, was calculated for each set of specimens using the equation

$$\bar{\sigma} = \frac{\sum_{i}^{n} \sigma_i \Delta t_i}{\sum_{i}^{n} \Delta t_i} \qquad \text{(Eq 1)}$$

where α_i is the stress in the *i*th layer of the coating calculated by the MLRM and Δt_i is the thickness of the *i*th layer. The average residual stress in the coating for each set of four specimens is shown in Table 5 along with the almen strip (type N)[8] result for each sprayed coating. The coatings are listed in order of increasing (more tensile) residual stress. Table 6 shows the residual stresses in each coating and the corresponding block volume loss when tested against Al-Ni-Bz blocks under a load of 6.8 kg. The table suggests that, if there is a relation between the residual stresses and the block volume loss, it is not a simple one. More study is needed to examine the possible relationships between the residual stress state in a coating and the coating's wear characteristics.

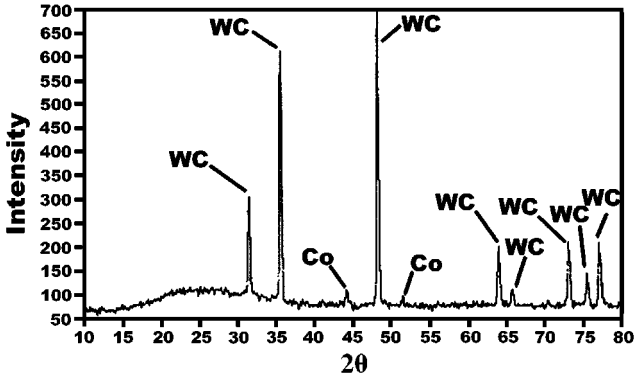

Fig. 8 X-ray spectra for starting powder 83WC-17Co

4.3 XRD Results

The phase compositions of the feedstock powders and of the HVOF sprayed coatings were investigated by XRD using CuK_α radiation in the range $2\theta = 10$ to 80°. The three feedstock powders used to produce the coatings listed in Table 4 were analyzed to determine the characteristics of the powder before spraying. Figure 8 shows the diffraction pattern for the 83WC-17Co powder used for the coatings that were sprayed according to three residual stress targets—high compressive, low compressive, and tensile. The WC and small amounts of free cobalt were identified in the diffraction patterns. There was no evidence of W_2C or elemental tungsten (W) in any of the feedstock powder analyses.

Figure 9 shows the diffraction patterns for the 83WC-17Co high compressive residual stress, low compressive residual stress, and tensile residual stress coatings. All coatings show strong WC components, which are desirable for good wear characteristics. But, they also indicate the presence of elemental tungsten (W), the compound αW_2C, and broad maxima in the 38 to 46° two-theta range, which is characteristic of microcrystalline or amorphous material (probably Co).

According to Nerz *et al.*,[9] a coating must retain a large volume fraction of finely distributed tungsten monocarbide (WC) to achieve optimum wear properties. Retaining a large WC fraction requires minimizing the decarburization of WC, which can occur at the high temperatures associated with the thermal spraying process according to the following reactions:

$$2WC \rightarrow W_2C + C \qquad \text{(Eq 2)}$$

$$W_2C \rightarrow 2W + C \qquad \text{(Eq 3)}$$

These reactions are time and temperature dependent.

The amorphous material indicated by the broad maxima in Fig. 9 is likely created by the diffusion of carbon and tungsten into the cobalt matrix and the subsequent rapid solidification typical of thermal spray processes. Cobalt, excess carbon, and some tungsten are thus present in the coatings in the amorphous state. Carbon and tungsten that have diffused into the cobalt matrix, therefore, are not available to form WC. Furthermore, the cobalt matrix in an amorphous state may not be as effective as the elemental crystalline cobalt as a binder for the WC particles.

The x-ray spectra shown in Fig. 9 are ordered according to worst wear characteristics (high compressive residual stress tar-

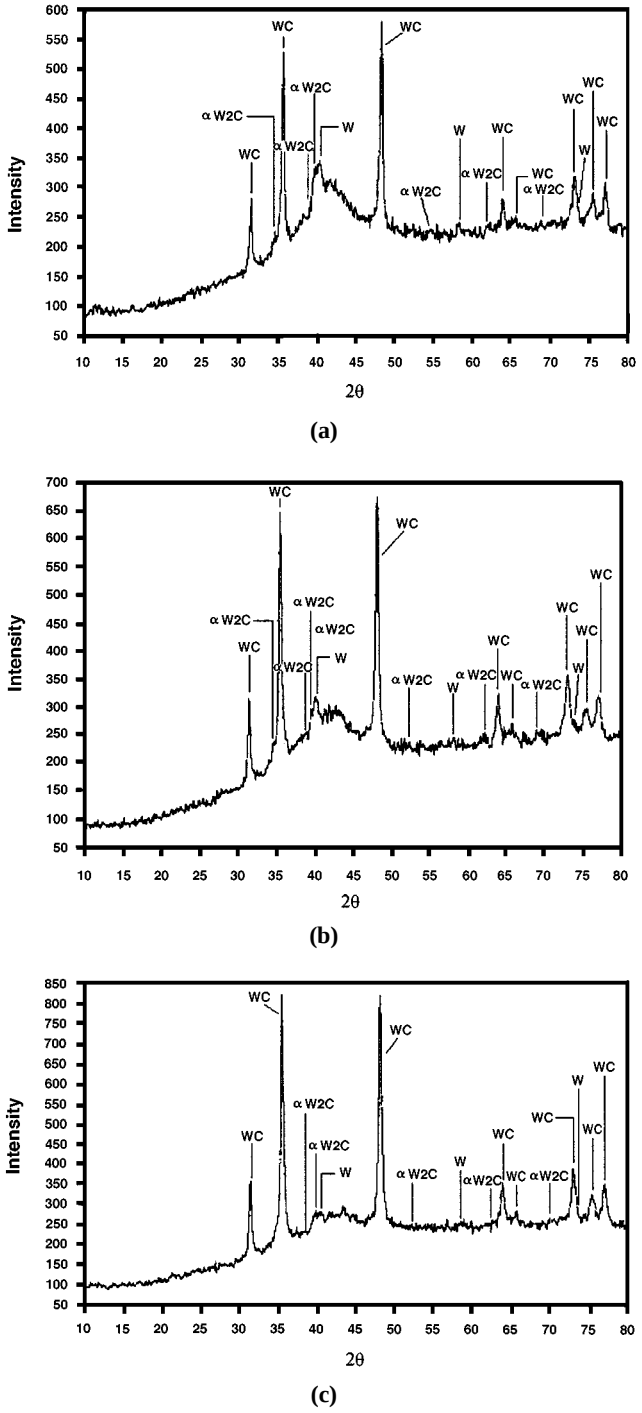

Fig. 9 X-ray spectra for three HVOF coatings: (**a**) 83WC-17Co high compressive residual stress, (**b**) 83WC-17Co low compressive residual stress, and (**c**) 83WC-17Co tensile residual stress

get) to best wear characteristics (tensile residual stress target). By comparing the heights of the broad maxima representing amorphous material to the heights of the WC peaks in each of the three figures, one can observe that better wear performance in the coatings tested corresponds to less amorphous material in the coating.

In order to obtain a semiquantitative indication of the extent of powder decarburization during spraying and of the extent of

Table 6 Average residual stresses in the coatings and volume loss in the Al-Ni-Bz blocks(a)

Coating material	Average residual stress, MPa	Block volume loss (6.8 kg Al-Ni-Bz), 10^{-3} mm^3
86WC-10Co-4Cr	270 (C)	66.2
83WC-17Co (high compressive residual stress)	169.3 (C)	538.5
88WC-12Co HVOF	138 (C)	358.7
83WC-17Co (low compressive residual stress)	100 (C)	159.8
83WC-17Co (tensile residual stress)	71 (T)	101.2
88WC-12Co plasma	160 (T)	299.3
Chrome	234 (T)	177.4

(a) T—tension, and C—compression

Table 7 XRD peak height ratio (W_2C/WC) for the coatings

Coating type	Crystalline compounds present	(αW_2C/WC)	Block volume loss (6.8 kg Al-Ni-Bz), 10^{-3} mm^3
83WC-17Co, high compressive residual stress	WC, W, αW_2C	0.23	538.5
88WC-12Co, HVOF	WC, W, αW_2C	0.15	358.7
83WC-17Co, low compressive residual stress	WC, W, αW_2C	0.14	159.8
83WC-17Co, tensile residual stress	WC, W, αW_2C	0.04	101.2

retention of WC, the ratios of the peak height of αW_2C (at d = 2.275 Å) to the peak height of WC (at d = 1.884 Å) were computed for each coating and are provided in Table 7 along with block wear data for each coating. Lower αW_2C/WC peak ratios indicate lesser degrees of decarburization. Smaller block volume losses indicate better block wear performance. This table indicates that a lesser degree of decarburization during deposition corresponds to better wear performance for the coating.

4.4 SEM Results

A micrograph of a region within the scar produced by the 83WC-17Co high compressive residual stress coated ring against the 83WC-17Co high compressive residual stress coated block (Fig. 10a) reveals removal of WC particles during the wear test (pullout) to a greater extent than when compared to a similar region within the scar produced by the 83WC-17Co low compressive residual stress coated ring against the 83WC-17Co low compressive residual stress coated block (Fig. 10b). Perhaps the greater fraction of amorphous material in the high compressive residual stress coating reduced the effectiveness of the cobalt matrix as a binder for the WC particles in this coating.

Figure 11 shows the top view of the 83WC-17Co high compressive residual stress coating and the 83WC-17Co low

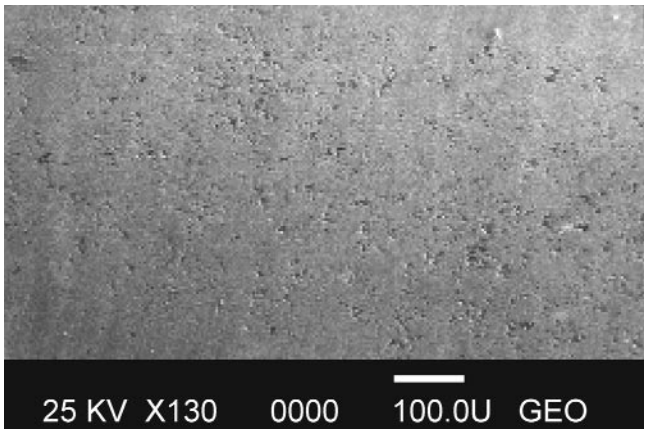

(a)

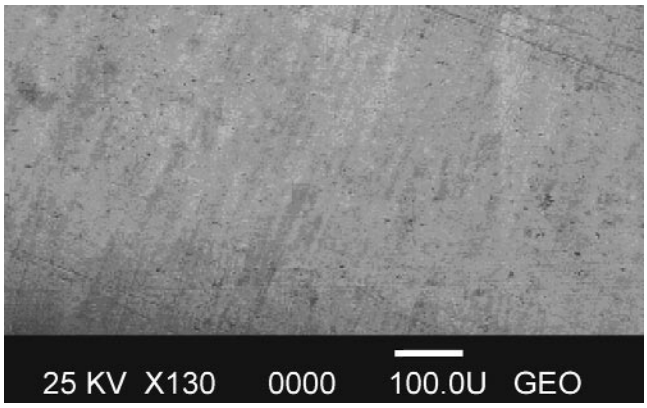

(b)

Fig. 10 Secondary electron image of a region within the scar produced in two HVOF coated blocks: (**a**) 83WC-17Co high compressive residual stress coated block tested against 83WC-17Co high compressive residual stress coated ring and (**b**) 83WC-17Co low compressive residual stress coated block tested against 83WC-17Co low compressive residual stress coated ring

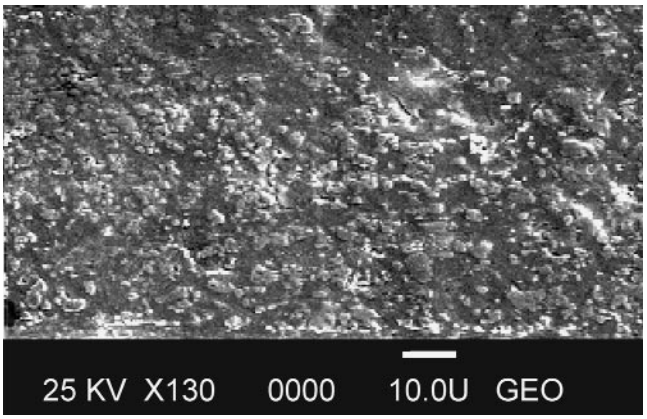

(a)

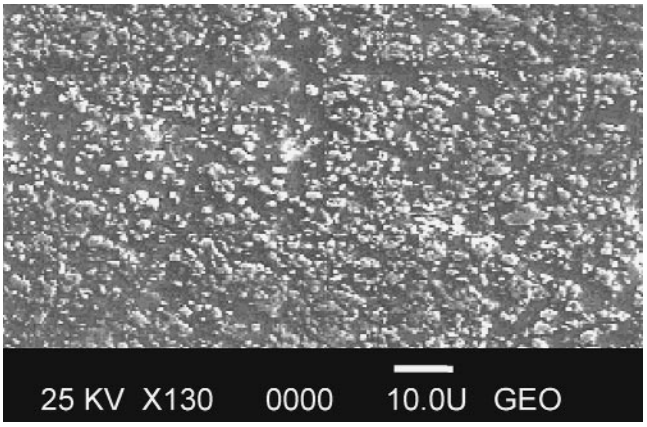

(b)

Fig. 11 Secondary electron image showing the density of WC particles (in relief) in the top layer of two HVOF coatings: (**a**) 83WC-17Co high compressive residual stress coating and (**b**) 83WC-17Co low compressive residual stress coating

compressive residual stress coating. These representative micrographs reveal that the volume fraction of finely distributed WC particles is higher in the low compressive residual stress coating than in the high compressive residual stress coating. All the HVOF coatings had very low porosities. The 83WC-17Co tensile residual stress coating having virtually no voids was one of the best performing coatings in all three types of wear tests conducted in this research.

4.5 Young's Modulus and Microhardness of Coatings

The elastic moduli (E_c) and the Poisson's ratio of the coatings were determined by CBBM, and the results are shown in Table 8 with the microhardness of the coatings.

5. Conclusions

Sliding wear characteristics of WC thermal spray coatings and electroplated chrome tested against Al-Ni-Bz blocks, Cu-Be blocks, and against themselves were studied. Results show that the HVOF 83WC-17Co tensile residual stress level coatings, HVOF 86WC-10Co-4Cr coatings, and HVOF 83WC-17Co low compressive residual stress level coatings performed better than chrome plating when tested against Al-Ni-Bz blocks. The HVOF 83WC-17Co high compressive residual stress coatings, which had better fatigue characteristics than the chrome plating, did not perform well in wear when tested against the Al-Ni-Bz blocks. The HVOF 86WC-10Co-4Cr coatings and the HVOF 83WC-17Co tensile residual stress level coatings performed better in wear than chrome plating when tested against Cu-Be blocks. The chrome plating did not perform well in the self-tests. All of the WC-Co coatings except for the HVOF 83WC-17Co high compressive residual stress coating and HVOF 86WC-10Co-4Cr coating had better wear characteristics than chrome plating in self-tests.

The through-thickness residual stress measurements and the wear test results do not indicate a simple correlation between the sliding wear characteristics of the coating and the residual stresses in the coating. The XRD and SEM examinations suggest that other factors such as decarburization, volume percent

Table 8 Young's modulus, Poisson's ratio, and microhardness of the coatings

Coating material	Young's modulus, GPa	Poisson's ratio	Knoop hardness (500 gf)
83WC-17Co, tensile residual stress level	219.42	0.17	1175.8
83WC-17Co, low compressive residual stress level	233.2	0.25	1270.5
83WC-17Co, high compressive residual stress level	235.9	0.31	1253.7
88WC-12Co, HVOF	235.4	0.28	1276.2
86WC-10Co-4Cr	199.41	0.2	1281.9
Chrome electroplate	108.5	0.088	888.2
88WC-12Co, plasma	150.4	0.21	1144.9

and distribution of hard particles, and porosity may more strongly influence wear behavior than residual stresses. The degree of decarburizaton, the density of hard particles, coating porosity, and coating residual stresses depend on many factors including the equipment, powder, and spray parameters. Some coating application processes can produce highly compressive residual stresses in WC coatings. These coatings offer good fatigue performance. Other spray conditions provide coatings offering good wear characteristics but not necessarily highly compressive residual stresses. Thus, there is a need for research to identify WC coating systems that offer both superior fatigue characteristics (highly compressive residual stresses) and superior wear characteristics in the same coating.

Acknowledgments

The authors gratefully acknowledge the financial support from the Oklahoma Center for the Advancement of Science and Technology (OCAST) and Southwest Aeroservice, Inc. (Tulsa, OK). The authors also acknowledge the contributions of Mr. Ed Bowers, who designed and built the wear test machine, and Mr. Mohammed Muzzahir, for his contribution toward generating the experimental data.

References

1. B.E. Bodger, D.A. Somerville, W.A. Emery, and R.T.R. McGrann: *J. AESF*, 1997, vol. 84 (9).
2. R.T.R. McGrann, E.F. Rybicki, J.R. Shadley, D.J. Greving, W.A. Emery, D.A. Somerville, and B.E. Bodger: in *Thermal Spray: Meeting the Challenges of the 21st Century*, Christian Coddet, ed., ASM International, Materials Park, OH, 1998, vol. 1, pp. 557-62.
3. Anon: *ASTM Designation G77-Standard Test Method for Ranking Resistance of Materials to Sliding Wear Using Block-on-Ring Wear Test*, ASTM, Philadelphia, PA, 1993.
4. Anon: *Boeing Materials Specifications BMS 3-33-Grease*, The Boeing Company, Seattle, WA.
5. Anon: *DoD Military Specification QQ-C-320B-Chromium Plating (Electrodeposited)*, Defense Technical Information Center, Fort Belvoir, VA, 1987.
6. D.J. Greving, E.F. Rybicki, and J.R. Shadley: *J. Thermal Spray Technol.*, 1994, vol. 3 (4), pp. 379-88.
7. E.F. Rybicki, J.R. Shadley, Y. Xiong, and D.J. Greving: *J. Thermal Spray Technol.*, 1995, vol. 4 (4), pp. 377-83.
8. Anon: *SAE Specification AMS S13165-Shot Peening of Metal Parts*, SAE World Headquarters, Warrendale, PA.
9. J. Nerz, B. Kushner, and A. Rotolico: *J. Thermal Spray Technol.*, 1992, vol. 1 (2), pp. 147-52.